forests

MDPI

Article

Deterioration of Microstructures and Properties in Ancient Architectural Wood from Yingxian Wooden Pagoda (1056 AD) during Natural Aging

Keying Long, Kaiqiang Chen, Lanying Lin *, Feng Fu and Yong Zhong

Research Institute of Wood Industry, Chinese Academy of Forestry, Beijing 100091, China
* Correspondence: linly@caf.ac.cn; Tel.: +86-10-6288-9100

Abstract: The Yingxian Wooden Pagoda (1056 AD), located in Shanxi province, China, is a unique architectural pure-wooden artifact standing for a millennium. Despite its longevity, the structures and properties of the ancient architectural woods used in its construction have been significantly degraded due to long-term natural aging, which has profoundly impacted the preservation of this valuable cultural heritage. To better understand this degradation, we studied the deterioration of a baluster (*Larix principis-rupprechtii* Mayr.) from Yingxian Wooden Pagoda. The study employed various analytical techniques, including optical microscopy, atomic force microscopy, Fourier-transform infrared spectroscopy, solid-state ^{13}C nuclear magnetic resonance spectroscopy, X-ray diffraction, and nanoindentation technology, to evaluate the microstructures and properties of the ancient architectural woods. Results indicated that the destruction of wood cell walls was primarily transverse transwall destruction and interfacial debonding and that the degradation of chemical components was primarily in the hemicellulose (xylan) and amorphous region of cellulose. The reduced elastic modulus and hardness of tracheid cell walls in the ancient architectural woods were higher than in recent larch woods. This study would help deepen understanding of wood deterioration during long-term natural aging for the subsequent preservation and protection of wooden cultural heritages and longer use of ancient timber constructions.

Keywords: Yingxian Wooden Pagoda; natural aging; ancient architectural wood; deterioration; wood cell wall

Citation: Long, K.; Chen, K.; Lin, L.; Fu, F.; Zhong, Y. Deterioration of Microstructures and Properties in Ancient Architectural Wood from Yingxian Wooden Pagoda (1056 AD) during Natural Aging. *Forests* **2023**, *14*, 393. https://doi.org/10.3390/f14020393

Received: 4 January 2023
Revised: 8 February 2023
Accepted: 13 February 2023
Published: 15 February 2023

1. Introduction

Wood, a natural and organic biomaterial, has been extensively utilized in human life for thousands of years in various applications, including in tools, furniture, vehicles, weapons, and architecture [1–4]. Ancient timber constructions, as architectural wooden artifacts, are of exceptional historical, cultural, anthropological, economic, artistic, archaeological, and scientific value [2,4–7]. The Yingxian Wooden Pagoda (1056 AD), located in Shanxi province, China, is a particularly remarkable example, as it is the oldest and highest extant pure-wooden structure in the world, with a height of 67.58 m (Figure 1a) [3,5,8]. It has attracted extensive attention and research due to the mystery of standing for a millennium [3,8–12].

The mechanical properties of wood are closely correlated with the orientation of cellulose microfibrils, particularly in the dominant secondary 2 (S_2) layer of tracheids (softwoods) or fibers (hardwoods), as well as the composition and arrangement of its main chemical components, including cellulose microfibrils embedded in a matrix of hemicellulose and lignin [13–15]. As the sole building material used in Yingxian Wooden Pagoda, wood is susceptible to degradation due to natural aging [5,14], weathering [16], biodegradation [5,16,17], and other environmental and human factors [4], which pose a significant challenge to the preservation of ancient timber constructions [14]. The natural aging of wood refers to the normal degradation process that occurs after the wood has

been cut down in the absence of other accelerating effects [18]. Although ancient architectural woods in ancient timber constructions appear well-preserved, the morphological structures [19], chemical components [19], cellulose crystalline structures [20], and mechanical properties [21] of wood cell walls inevitably deteriorate significantly over time due to the single or combined action of UV irradiation, oxygen, humidity, temperature, and atmospheric pollutants [18].

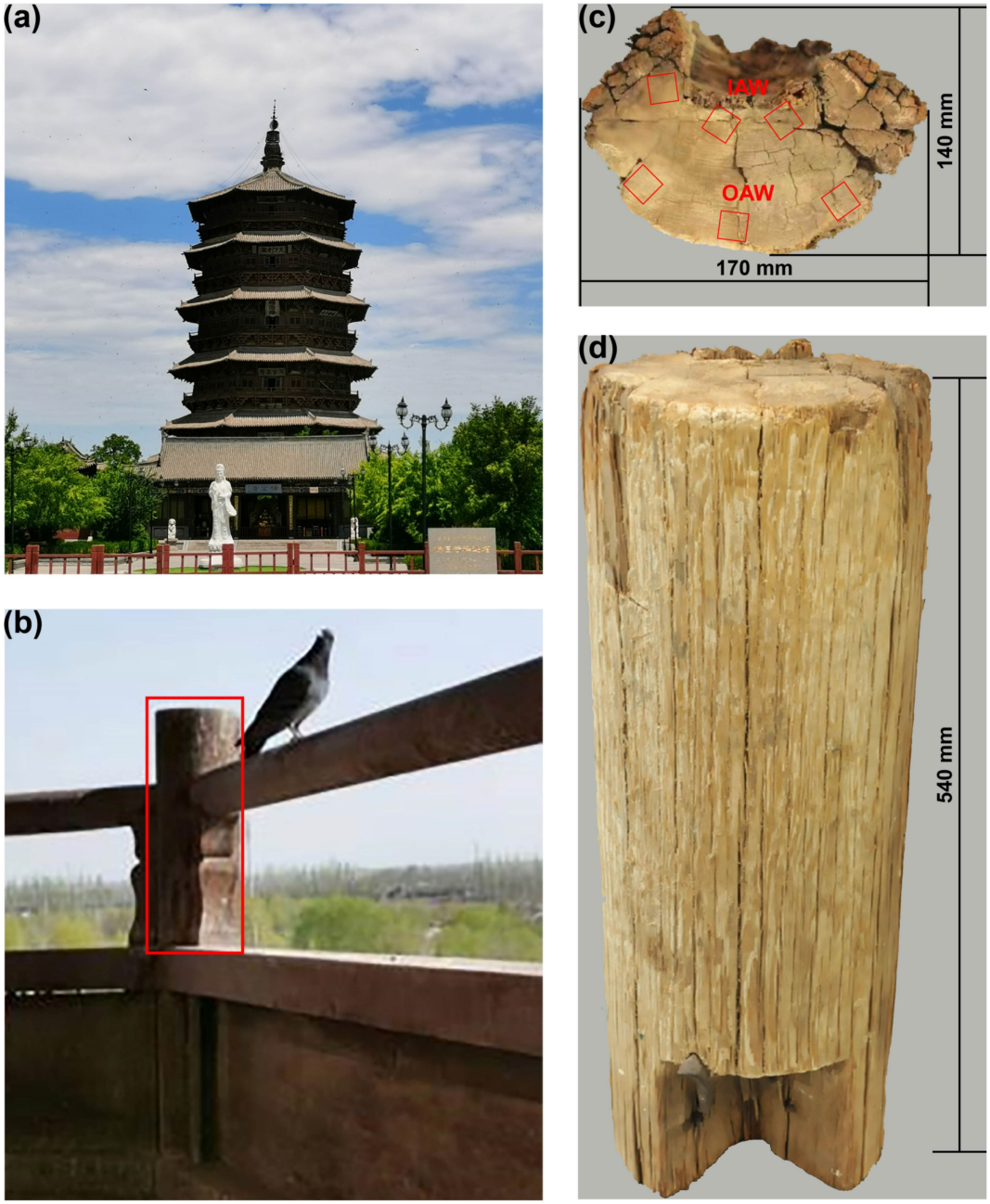

Figure 1. (**a**) Photograph of Yingxian Wooden Pagoda. (**b**) Photograph of a baluster in the red box. (**c**) The cross-section of the baluster. (**d**) The baluster was replaced from (**b**). IAW was collected from the inner part of the baluster; OAW was collected from the outer part of the baluster.

A study of archaeological elm wood from Chenghuang Temple, China, approximately 350 years old, showed a significant decrease in polysaccharide and lignin content, deterioration of microstructures, and changes in the micromechanical properties of cell walls at the outer part of the wood during natural aging [5]. Changes in environmental humidity

caused hygroexpansion of wood cell walls, leading to changes in the cell dimensions over time, slow hydrolysis of polysaccharides, oxidation of lignin, and leaching of degraded products and extractives from cell walls [4]. The combination of UV irradiation and oxygen rapidly depolymerizes hemicellulose and the amorphous region of cellulose, as well as oxidizing lignin [4]. The impact of environmental factors or application sites on changes in the chemical components of archaeological woods has been studied. Łucejko et al. investigated the deterioration processes induced by the burial environment of archaeological oak wood, suggesting that only a small amount of polysaccharides, mainly hemicellulose, underwent a chemical transformation during burial [22]. Analysis of the chemical components and micromechanical properties of load-bearing archaeological oak wood in the Oseberg Viking ship showed that although hemicellulose and the amorphous region of cellulose were significantly degraded in the archaeological wood, the longitudinal micromechanical properties of cell walls in the archaeological wood were increased by nanoindentation testing [23].

This study hypothesizes that the ancient architectural wood and recent larch wood will exhibit differences in microstructures and chemical components in wood cell walls, and therefore, their physical and mechanical properties will differ. This study aims to investigate the deterioration of microstructures and properties in the ancient architectural wood taken from the upper part of a baluster in the Yingxian Wooden Pagoda (1056 AD) located in Shanxi province, China (Figure 1b–d), where the annual average temperature is 1.84 °C with a minimum of −15.20 °C in December and a maximum of 15.55 °C in July, and the annual average environmental humidity is 52.8% with a minimum of 36.2% in March and a maximum of 68.2% in August [8]. The ancient architectural wood has been identified microscopically as larch wood (*Larix principis-rupprechtii* Mayr.), as reported previously [3], and shows many cracks due to long-term natural aging. The deterioration of microstructures and properties of the ancient architectural wood was studied using various characterization techniques, including optical microscopy and atomic force microscopy (AFM) to investigate the destruction degree of cell wall structures, Fourier-transform infrared (FTIR) spectroscopy, and solid-state ^{13}C nuclear magnetic resonance (NMR) spectroscopy to evaluate the degradation of chemical components in the cell walls, X-ray diffraction (XRD) to determine changes in cellulose crystalline structures, and nanoindentation testing to study the mechanical properties of cell walls at the nanometer level. A clear understanding of the deterioration in the microstructures and properties of ancient architectural wood during long-term natural aging is crucial for developing protection technology for the wooden cultural heritage and the continued use of ancient timber constructions.

2. Materials and Methods

2.1. Materials

An ancient wooden baluster from the Yingxian Wooden Pagoda (1056 AD), provided by the Chinese Academy of Cultural Heritage, was used for the research. The age of the ancient architectural wood was estimated to be 108 years, based on its size and the average width of its growth ring, which was determined to be 1.6 mm from limited samples. As a reference, a 35-year-old recent larch (*Larix principis-rupprechtii* Mayr.) wood was used from the Saihanba Forest in Chengde City, Hebei province, China. For the ancient architectural wood, three positions in its outer and inner parts were sampled for repeated measurements (Figure 1c). Similarly, for the recent larch wood, three positions in its sapwood and heartwood were sampled for repeated measurements. The sapwood of the recent larch wood (SRW) was used as the reference for the outer part of the ancient architectural wood (OAW), while the heartwood of the recent larch wood (HRW) was used as the reference for the inner part of the ancient architectural wood (IAW). All samples were stored under laboratory conditions before testing.

2.2. Transversal Microscopical Structure Analysis

Wood samples were transversely sliced using a sliding microtome (SM2010R, Leica, Baden-Württemberg, Germany) with a section thickness of 20 μm. The sections were stained with a 1% safranin solution and observed under an optical microscope (CX31, Olympus, Tokyo, Japan) at a magnification of 400×.

2.3. AFM Analysis

The wood samples with dimensions of $1 \times 1 \times 2\,mm^3$ (Radial × Tangential × Longitudinal, R × T × L) were embedded with SPI-PON™ 812 resin, which was polymerized in an oven at 60 °C until solidification. The embedded samples were then cut perpendicular to the fiber direction using an ultramicrotome (Ultracut UCT, Leica, Baden-Württemberg, Germany) equipped with a diamond knife (Diatome, Nidau, Switzerland) to produce a $1 \times 1\ mm^2$ smooth surface for AFM investigation. The tracheid cell walls ultrastructures were examined using an AFM (Dimension Edge, Veeco, New York, NY, USA) equipped with a standard tapping mode probe (RTESP-300, Veeco, New York, NY, USA). The cantilever length was 125 μm, and the resonance frequency was 300 kHz. The scanning rate was set at 0.5 Hz, and the images were captured with a digital resolution of 512 × 512 pixels and a scan size of $50 \times 50\ \mu m^2$. All data processing and image analysis were performed using Nanoscope Analysis software (Version 1.40, Bruker, Billerica, MA, USA).

2.4. FTIR Spectroscopy

The wood samples were ground into powders using a low-temperature grinder (935A, HATTIECS, Kirchlengern, Germany), and the resulting material was sieved through a 200-mesh screen. FTIR spectra of the dried powder samples were collected using an FTIR spectrometer (TENSOR 27, Bruker, Billerica, MA, Germany) in transmission mode. The spectra were obtained in the 4000–400 cm^{-1} wavenumber range, with 32 scans taken at a resolution of 4 cm^{-1}. The acquired spectra underwent baseline correction.

2.5. Solid-State ^{13}C NMR Spectrum Measurement

The dried powder samples underwent solid-state ^{13}C cross-polarization/magic-angle spinning (CP-MAS) NMR spectroscopy at room temperature using a solid-state NMR spectrometer (JNM-ECZ600R 600M, JEOL Japan Electronics Co., Ltd., Tokyo, Japan) equipped with a 3.2 mm tube. The ^{13}C Larmor frequency was 150.913 MHz. The spectra were obtained at a MAS frequency of 12 kHz, with 2000 scans accumulated and a relaxation delay of 2 s. The ^{13}C chemical shift was determined relative to the -CH_2 peak at 38.52 ppm of adamantane, which was an external reference for tetramethylsilane (TMS).

2.6. Determination of Main Chemical Components

The main chemical components of the wood samples, including lignin, cellulose, and hemicellulose, were determined using the standard approach outlined by the National Renewable Energy Laboratory (NREL, Golden, CO, USA) protocol [24].

2.7. Measurement of Relative Crystallinities

The relative crystallinities of the dried powder samples that had passed through an 80-mesh screen were determined using an X-ray powder diffractometer (D8 Advance, Bruker, Ettlingen, Germany) with Cu Kα_1 radiation. The instrument was operated at a voltage of 40 kV and a current of 40 mA, and the data was collected over a 2θ range of 5° to 40° with a step length of 0.05° and a scan rate of 0.1 °/s. The crystallinity index (C_rI) of the wood samples was calculated as follows [25]:

$$C_rI = \frac{I_{002} - I_{am}}{I_{002}} \times 100\% \quad (1)$$

where I_{002} is the maximum diffraction intensity of the 002 crystallographic planes at $2\theta \approx 22.4^{\circ}$ and I_{am} is the minimum diffraction intensity of the amorphous region of cellulose at $2\theta \approx 18.5$–19.2°.

2.8. Quasi-Static Nanoindentation Test

The mechanical properties of the tracheid cell walls of the wood samples were studied using a nanoindentation instrument (TI 950, Hysitron Inc., Minneapolis, MN, USA). The samples were first cut into cubes with dimensions of $7 \times 7 \times 15$ mm^3 (R × T × L), and a cross-section of about 1×1 mm^2 was then polished perpendicular to the fiber direction from the top of the cubes using the ultramicrotome equipped with the diamond knife. The polished samples were allowed to equilibrate in the chamber of the nanoindentation instrument for at least 4 h before testing.

The experiments were performed with a triangular pyramid diamond indenter (Ti-0039, Berkovich, Hysitron Inc., Minneapolis, MN, USA) and were carried out in a load-controlled mode with a peak indentation load of 150 μN. The loading and unloading time were set to 5 s, and the holding time was set to 2 s. A minimum of 20 indents were performed on the transverse sections of each sample. The reduced elastic modulus (E_r) and hardness (H) of the samples were calculated from the initial unloading stiffness (S), contact area (A) at peak indentation load, and peak indentation load (P_{max}) as follows [26]:

$$E_r = \frac{\sqrt{\pi}}{2\beta}\frac{S}{\sqrt{A}} \quad (2)$$

$$H = \frac{P_{max}}{A} \quad (3)$$

where β is a correction factor related to the geometry of the Berkovich indenter ($\beta = 1.034$).

2.9. Data Analysis

The FTIR spectra were analyzed using OPUS 8.5 software (Bruker Inc., Germany). The statistical significance of the differences between the wood samples was evaluated using Analysis of Variance (ANOVA) and Least-Significant-Difference (LSD) tests, performed with IBM SPSS Statistics software (Version 26, SPSS Inc., Armonk, NY, USA), with a 95% confidence interval of probability. The peak intensity ratios calculated from the average FTIR absorbance spectra, the relative crystallinities, as well as reduced elastic modulus and hardness of tracheid cell walls were analyzed.

3. Results and Discussion

3.1. Morphological Structure Analysis

The morphological characteristics of ancient architectural woods were investigated to evaluate the degree of deterioration using optical microscopy and AFM. In contrast to the integrity of cell structures in HRW, the morphology of cells in the earlywood of IAW showed moderate destruction after long-term natural aging, whereas the morphology of cells in the latewood of IAW showed no signs of destruction (Figure 2). AFM analysis revealed that the earlywoods of IAW and OAW showed moderate to severe destruction, while the latewoods of IAW and OAW showed slight destruction (Figure 3). The destruction of cell walls in ancient architectural woods was mainly transverse transwall destruction on radial cell walls and interfacial debonding. The transverse transwall destruction on radial cell walls occurred mainly at both ends of pits in earlywoods, propagating along the interface of cell walls, inducing interfacial debonding due to many pit structures in radial cell walls of earlywoods in softwoods [27–29]. In latewoods, with fewer pit structures, the transverse transwall destruction on radial cell walls was near cell corners, subsequently propagating along the interface of cell walls, inducing interfacial debonding. The results obtained from optical microscopy and AFM indicated that the microstructures of cell walls in the outer part of the ancient architectural wood were destructed, while there was less

destruction in the microstructures of cell walls in the inner part of the ancient architectural wood during long-term natural aging.

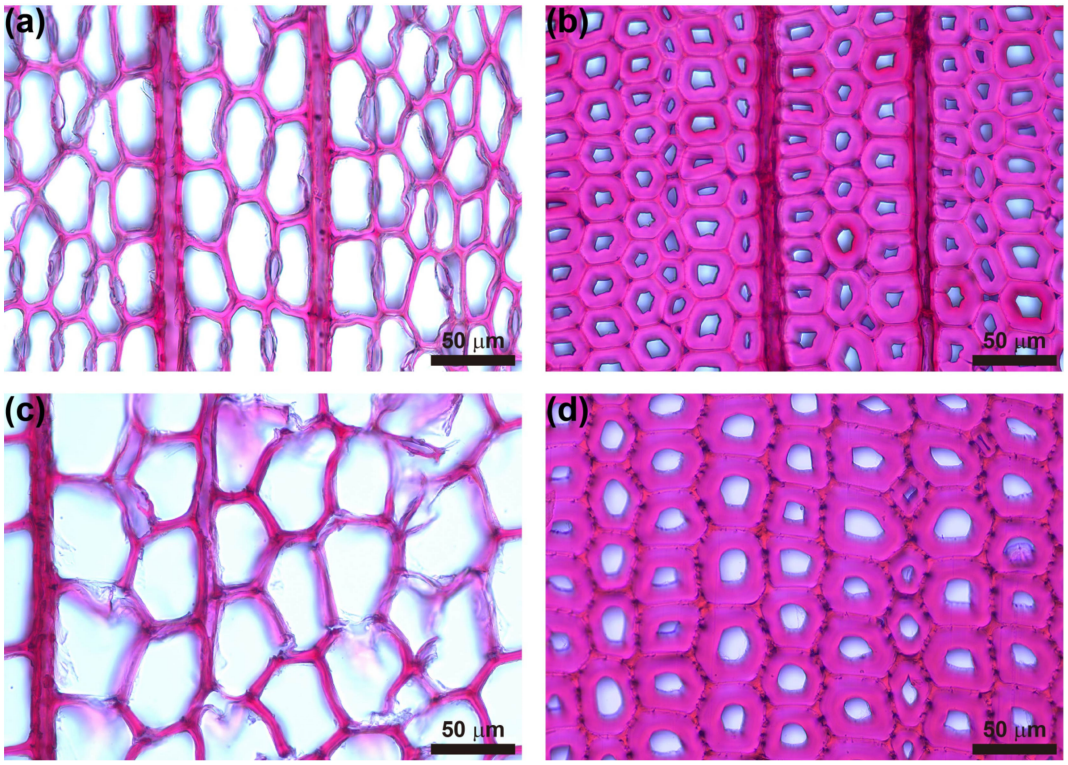

Figure 2. Optical micrographs taken from cross-sections of the heartwood of the recent larch wood (HRW) and the inner part of the ancient architectural wood (IAW). (**a**) The earlywood of HRW. (**b**) The latewood of HRW. (**c**) The earlywood of IAW. (**d**) The latewood of IAW.

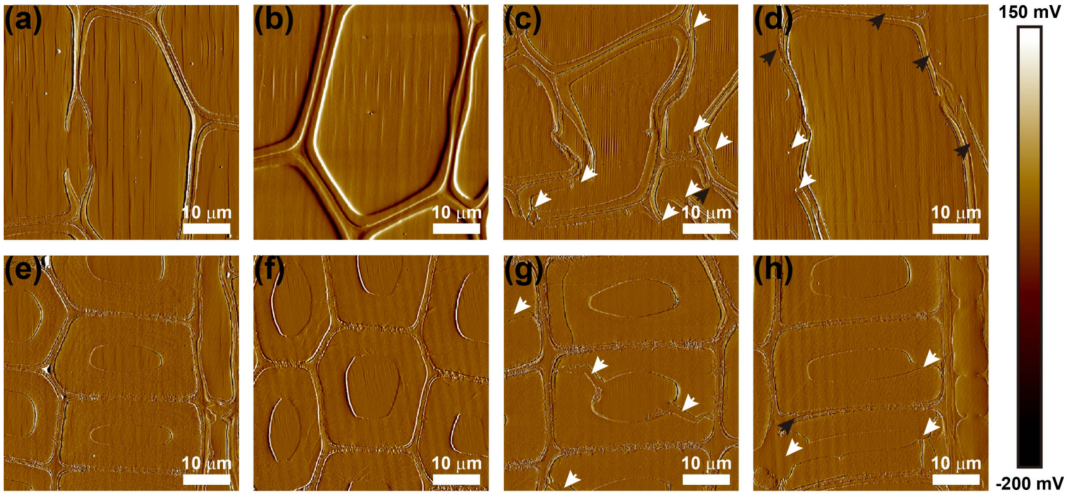

Figure 3. AFM images of cross-sections in recent larch woods and ancient architectural woods. (**a**) The earlywood of SRW. (**b**) The earlywood of HRW. (**c**) The earlywood of OAW. (**d**) The earlywood of IAW. (**e**) The latewood of SRW. (**f**) The latewood of HRW. (**g**) The latewood of OAW. (**h**) The latewood of IAW. The white arrows indicate transverse transwall destruction; the black arrows indicate interfacial debonding.

3.2. Chemical Components Analysis

The chemical composition of wood plays a crucial role in determining its mechanical properties [13]. In the case of ancient architectural woods, the chemical components can

undergo characteristic degradation over extended periods of natural aging. This study provides a comprehensive examination and comparison of the chemical components of both recent larch woods and ancient architectural woods (Figure 4).

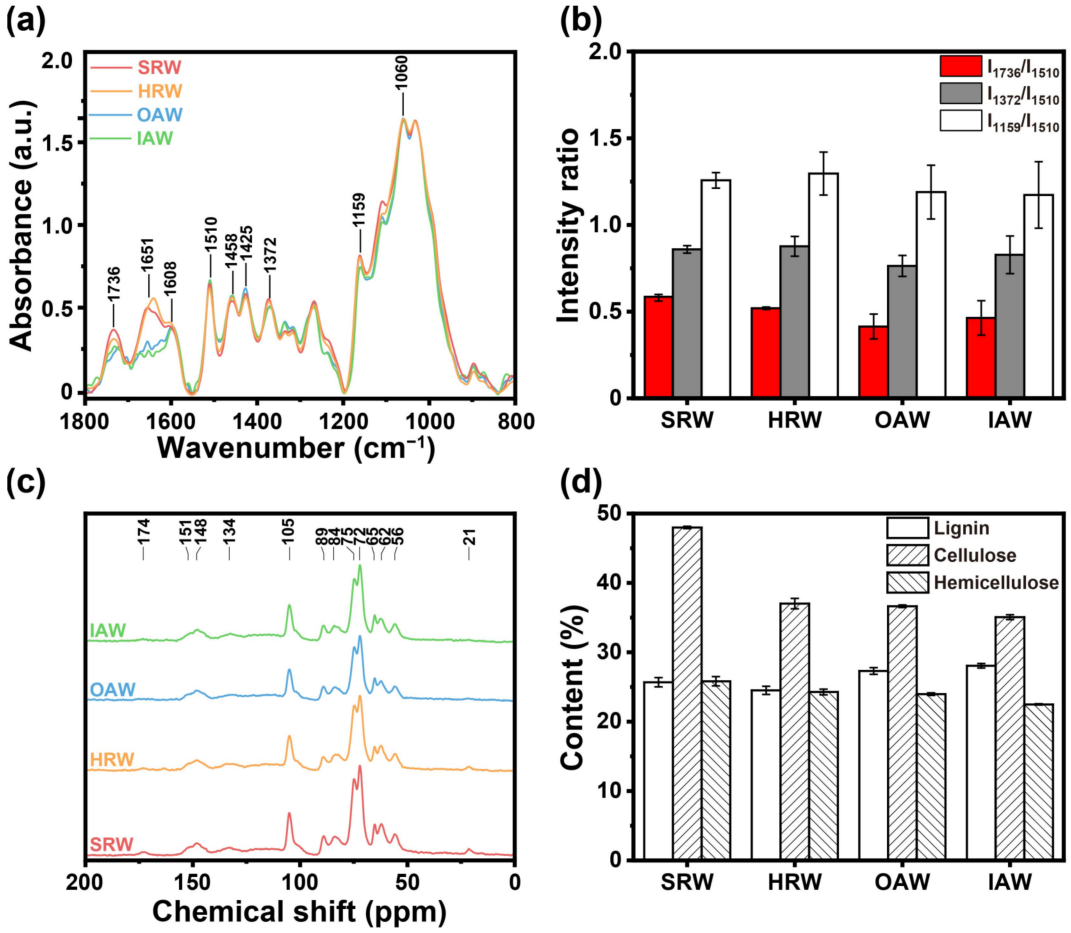

Figure 4. Chemical analysis of recent larch woods and ancient architectural woods. (**a**) Average FTIR absorbance spectra in 1800–800 cm^{-1}. (**b**) The relative intensity ratio of I_{1736}, I_{1372}, and I_{1159} versus I_{1510}. (**c**) Solid-state ^{13}C NMR spectra. (**d**) Contents of lignin, cellulose, and hemicellulose.

FTIR spectroscopy was employed to examine the difference of functional groups in the chemical components between recent larch woods and ancient architectural woods. The average FTIR absorbance spectra of recent larch woods and ancient architectural woods in the fingerprint region of 1800–800 cm^{-1} are shown in Figure 4a. All FTIR absorbance spectra were normalized at the highest absorbance intensity in the 1800–800 cm^{-1} region. The peak with the highest absorbance intensity of recent larch woods and ancient architectural woods was observed at 1060 cm^{-1}, corresponding to the stretching vibrations of C–O in polysaccharides [19]. The results showed that the intensities of the absorbance peaks at 1736 cm^{-1} (stretching vibrations of unconjugated C=O of the carbonyl, carboxyl, and acetyl groups in xylan, a component of hemicellulose), 1372 cm^{-1} (bending vibrations of C–H in polysaccharides), and 1159 cm^{-1} (asymmetric stretching vibrations of C–O–C in polysaccharides) were reduced in ancient architectural woods compared to recent larch woods, indicating partial depletion of polysaccharides, particularly hemicellulose, in ancient architectural woods [1,13,14,19,20,30–34]. On the other hand, the intensities of the absorbance peaks at 1608 cm^{-1} (stretching vibrations of the aromatic skeleton combined with the stretching vibrations of C=O in lignin), 1510 cm^{-1} (stretching vibrations of the aromatic skeleton in lignin), 1458 cm^{-1} (asymmetric bending vibrations of C–H of $–CH_3$ and $–CH_2$ groups in lignin), and 1425 cm^{-1} (stretching vibrations of the aromatic skeleton

combined with in-plane bending vibrations of C–H in lignin) were either similar or slightly increased in ancient architectural woods, indicating well preservation of lignin during long-term natural aging [1,13,14,19,20,31–33,35]. However, the peak at 1651 cm^{-1} for oxidized lignin units with carbonyl groups at C_α was absent in the spectra of ancient architectural woods, indicating degradation of the side chains in lignin [33].

The relative changes in polysaccharides and lignin were calculated using the relative intensity ratios of the peaks at 1736, 1372, and 1159 cm^{-1} assigned to the hemicellulose, polysaccharides (including hemicellulose and cellulose), and crystalline regions in cellulose against the peak at 1510 cm^{-1} assigned to lignin [20] (Figure 4b). For recent larch woods, the value of the hemicellulose to lignin ratio in the SRW was significantly higher than that in the HRW, while there was no significant difference between the SRW and the HRW for the ratios I_{1372}/I_{1510} and I_{1159}/I_{1510}. The ancient architectural woods showed no significant difference between the OAW and the IAW for the ratios I_{1736}/I_{1510}, I_{1372}/I_{1510}, and I_{1159}/I_{1510}. The results revealed that the degradation was primarily in hemicellulose (xylan), and the degradation in the outer part of ancient architectural wood was more serious than in the inner part during long-term natural aging.

The solid-state ^{13}C CP-MAS NMR spectra were used to investigate the deterioration of the chemical structures of ancient architectural woods over time (Figure 4c). The results showed that the signals at 21 ppm and 172 ppm assigned to the $–CH_3$ of acetyl groups in hemicellulose and carbonyl groups of polysaccharides almost disappear in ancient architectural woods, suggesting cleavage of these groups in the side chains of hemicelluloses [31,32]. Additionally, the intensity ratios of signals at 89 ppm and 84 ppm assigned to C_4 crystalline and amorphous regions of cellulose increased, and the intensity ratios of signals at 65 ppm and 62 ppm ascribed to C_6 crystalline and amorphous regions of cellulose also increased, indicating degradation of the amorphous region of cellulose and a more ordered arrangement of crystalline cellulose [2,32,36–39]. For recent larch woods, the intensity ratio of the signal at 151 ppm and 148 ppm attributed to etherified and non-etherified aromatic carbons in lignin in SRW (0.72) was similar to that in HRW (0.71), while for ancient architectural woods, the intensity ratio of these signals was found to be lower in OAW (0.63) compared to IAW (0.71), pointing to depletion of the β-O-4 interlinks in the outer part of the ancient architectural wood during long-term natural aging [32,37]. The intensity ratios of the signal at 75 ppm assigned to C–OH in the β-O-4 linked side chain of lignin against the signal at 72 ppm ascribed to $C_{2,3,5}$ decreased in ancient architectural woods compared to recent larch woods, suggesting breakage of β-O-4 interlinks in lignin in ancient architectural woods during long-term natural aging [31].

The degradation degree of ancient architectural woods was estimated by quantitatively assessing residual chemical components on wood cell walls in ancient architectural woods compared to recent larch woods (Figure 4d). For recent larch woods, the lignin contents showed no significant difference between the sapwood and the heartwood, while the cellulose and hemicellulose contents in the sapwood were significantly higher than that in the heartwood due to the high content of extractives in the heartwood [40,41]. Compared with the HRW, the cellulose and hemicellulose contents in SRW increased by 30% and 6%, respectively. For ancient architectural woods, the contents of the main chemical components showed a similar tendency from the outer to the inner part to that of recent larch woods. The lignin contents showed no significant difference between OAW and IAW, while the cellulose and hemicellulose contents in OAW were significantly higher than in IAW. Compared with IAW, the contents of cellulose and hemicellulose in OAW increased by 5% and 7%, respectively. The results indicated that the cellulose in the outer part of the ancient architectural wood was seriously degraded.

All the above results indicated that during long-term natural aging, the polysaccharides, particularly hemicellulose and the amorphous region of cellulose, in the ancient architectural wood have partially degraded, while no obvious changes in the lignin were observed.

3.3. Cellulose Crystalline Structure Analysis

The cellulose crystalline structures of recent larch woods and ancient architectural woods were studied by XRD [42]. The X-ray diffractograms of recent larch woods and ancient architectural woods are presented in Figure 5a. All samples displayed typical patterns of native cellulose Iβ with broad diffraction bands from 14.8° to 16.8° (101 and 10$\bar{1}$ crystallographic planes) and high-intensity diffraction bands at 2θ = 22.4° (002 crystallographic planes) [20,43–47]. However, the intensities of the diffraction bands differed, indicating changes in relative crystallinities [20]. The HRW presented low-intensity crystalline diffraction bands compared with other samples, indicating that the relative crystallinity was lower than those of other samples. The relative crystallinities of recent larch woods and ancient architectural woods were determined (Figure 5b). The relative crystallinity of recent larch woods was found to be significantly higher in SRW (45.64%) compared to HRW (34.67%), while for ancient architectural woods, the increase in crystallinity in IAW (46.21%) was attributed to the depletion of amorphous polysaccharides resulting in the oriented arrangement of cellulose molecules during long-term natural aging. However, due to the initial depletion of amorphous polysaccharides followed by the crystalline cellulose in OAW during long-term natural aging, there was no significant difference in the relative crystallinities between OAW (46.65%) and IAW (46.21%) [3]. On the contrary, the study by Guo et al. found that the waterlogged archeological woods showed lower crystallinities than those of recent woods due to the depletion of polysaccharides and the modification of lignin, resulting in the disoriented arrangement of crystalline cellulose [32].

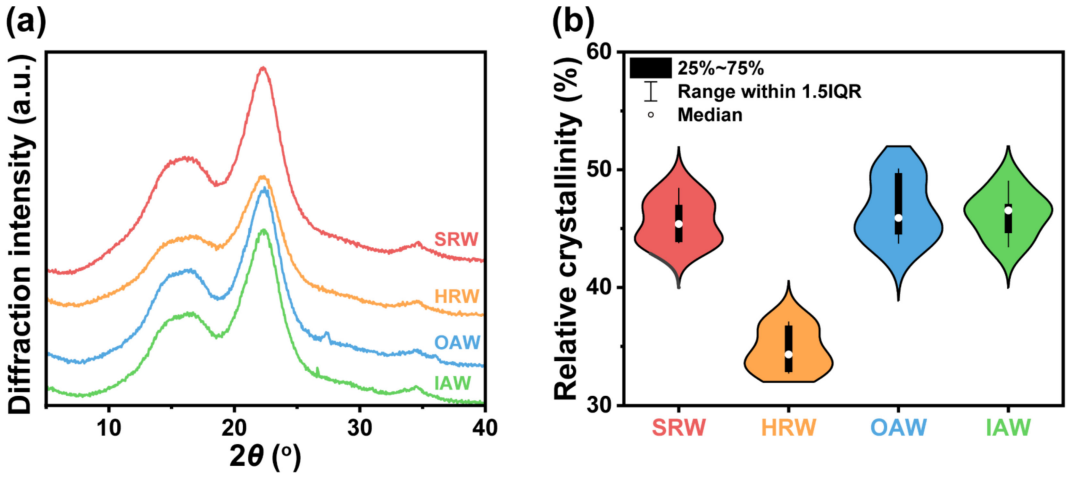

Figure 5. The cellulose crystalline structures of recent larch woods and ancient architectural woods. (**a**) X-ray diffractograms. (**b**) The relative crystallinities.

3.4. Micromechanical Properties

Nanoindentation technology is considered an effective and micro-destructive means to test the micromechanical properties of wood at the nanometer level, including elastic modulus, viscoelastic, and creep properties [5,15,31,48,49]. This study applied quasi-static nanoindentation to examine the longitudinal micromechanical properties of tracheid cell walls in both recent larch woods and ancient architectural woods without resin embedding, avoiding the influence of the embedded resin to provide a more accurate assessment of the tracheid cell walls [31]. Since the S_2 layer is the thickest layer of cell walls (more than 80%) and has a dominant impact on the longitudinal mechanical properties of wood cell walls [15,31,49], the study focused on the differences in micromechanical properties in the S_2 layer of tracheids between recent larch woods and ancient architectural woods (Figure 6). The results showed that the *Er* and hardness of sapwoods in recent larch wood were significantly lower than those of heartwoods ($p < 0.05$), and the *Er* and hardness of earlywoods were significantly lower than those of latewoods ($p < 0.05$). However, no significant difference was observed between the outer and inner parts of ancient architectural

wood in terms of *Er* and the hardness of latewoods. The hardness of earlywoods also showed no significant difference between the outer and inner parts of ancient architectural wood. The *Er* and hardness of ancient architectural woods were higher than those of recent larch wood, a phenomenon previously reported in archaeological oak and attributed to a loss of pectins and modification in the lignocellulosic cell wall polymers [23].

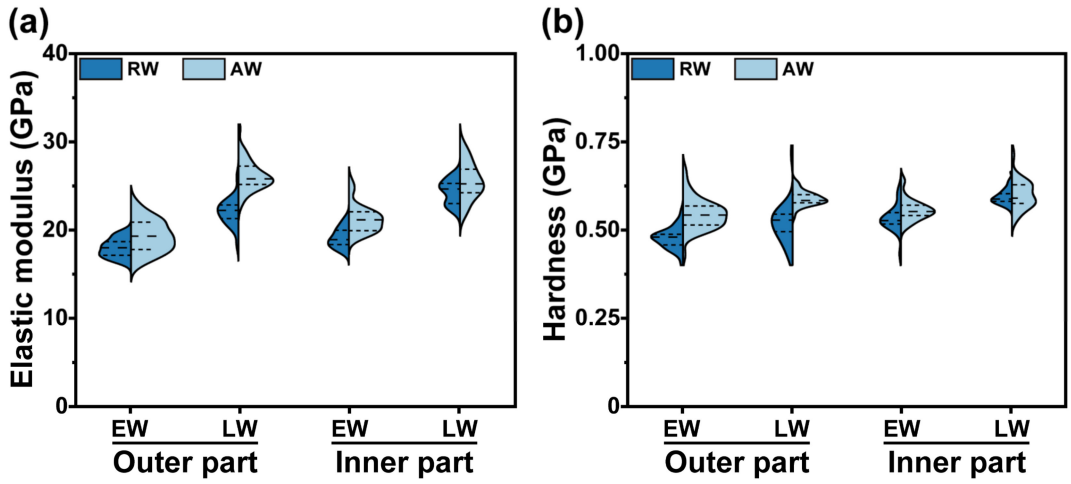

Figure 6. Reduced elastic modulus and hardness of the S_2 layer in tracheid cell walls of recent larch woods and ancient architectural woods. (**a**) Reduced elastic modulus. (**b**) Hardness.

4. Conclusions

In this study, a baluster dating back to Song Dynasty was procured and analyzed to understand the deterioration of microstructures and properties in ancient architectural wood during long-term natural aging. The results showed that the destruction of cell walls in ancient architectural woods was mainly transverse transwall destruction and interfacial debonding, with the outer part of the ancient architectural wood showing more obvious destruction than the inner part during long-term natural aging. The ancient architectural woods displayed a partial depletion of polysaccharides, particularly the amorphous regions (i.e., hemicellulose and amorphous region of cellulose), while no obvious change in lignin was observed after long-term natural aging. The observed deterioration differed for the sampling position in the log (outer or inner part) of ancient architectural woods. The deterioration did not negatively impact the longitudinal micromechanical properties of wood. These findings provide valuable insights into the deterioration of structures and properties in ancient architectural woods and have the potential to guide and improve preservation efforts for ancient wooden artifacts globally.

Author Contributions: Conceptualization, K.L., L.L. and Y.Z.; methodology, K.L., K.C. and L.L.; validation, K.L., K.C. and L.L.; formal analysis, K.L. and K.C.; investigation, K.L.; resources, Y.Z.; data curation, K.L.; writing—original draft preparation, K.L.; writing—review and editing, K.L. and L.L.; visualization, K.L.; supervision, L.L.; project administration, L.L.; funding acquisition, F.F. All authors have read and agreed to the published version of the manuscript.

Funding: This research was funded by the Chinese Academy of Forestry Fundamental Research Fund, grant number CAFYBB2020ZA003.

Data Availability Statement: Data are available upon request to the corresponding author.

Acknowledgments: The authors express their gratitude to Zhenrui Li and Dengkang Guo for their assistance with this study.

Conflicts of Interest: The authors declare no conflict of interest.

References

1. García-Iruela, A.; García Esteban, L.; García Fernández, F.; de Palacios, P.; Rodriguez-Navarro, A.B.; Sánchez, L.G.; Hosseinpourpia, R. Effect of degradation on wood hygroscopicity: The case of a 400-year-old coffin. *Forests* **2020**, *11*, 712. [CrossRef]
2. Huang, C.; Su, Y.; Shi, J.; Yuan, C.; Zhai, S.; Yong, Q. Revealing the effects of centuries of ageing on the chemical structural features of lignin in archaeological fir woods. *New J. Chem.* **2019**, *43*, 3520–3528. [CrossRef]
3. Mi, X.; Li, T.; Wang, J.; Hu, Y. Evaluation of salt-induced damage to aged wood of historical wooden buildings. *Int. J. Anal. Chem.* **2020**, *2020*, 8873713. [CrossRef] [PubMed]
4. Ghavidel, A.; Hosseinpourpia, R.; Militz, H.; Vasilache, V.; Sandu, I. Characterization of archaeological European white elm (*Ulmus laevis* P.) and black poplar (*Populus nigra* L.). *Forests* **2020**, *11*, 1329. [CrossRef]
5. Han, L.; Wang, K.; Wang, W.; Guo, J.; Zhou, H. Nanomechanical and topochemical changes in elm wood from ancient timber constructions in relation to natural aging. *Materials* **2019**, *12*, 786. [CrossRef]
6. Łucejko, J.J.; Tamburini, D.; Modugno, F.; Ribechini, E.; Colombini, M.P. Analytical pyrolysis and mass spectrometry to characterise lignin in archaeological wood. *Appl. Sci.* **2020**, *11*, 240. [CrossRef]
7. Zou, Z.; Zhao, X.; Zhao, P.; Qi, F.; Wang, N. CNN-based statistics and location estimation of missing components in routine inspection of historic buildings. *J. Cult. Herit.* **2019**, *38*, 221–230. [CrossRef]
8. Mi, X.; Meng, X.; Yang, Q.; Li, T.; Wang, J. Analysis of the residual deformation of Yingxian Wood Pagoda. *Adv. Civ. Eng.* **2020**, *2020*, 2341375. [CrossRef]
9. Deng, Y.; Li, Y.; Li, A. Seismic safety assessments of historical timber buildings using updated finite element models: Case study of Yingxian wooden pagoda, China. *J. Build. Eng.* **2023**, *63*, 105454. [CrossRef]
10. Sha, B.; Xie, L.; Yong, X.; Li, A. An experimental study of the combined hysteretic behavior of dougong and upper frame in Yingxian Wood Pagoda. *Constr. Build. Mater.* **2021**, *305*, 124723. [CrossRef]
11. Li, Y.; Sun, P.P.; Li, A.; Deng, Y. Wind effect analysis of a high-rise ancient wooden tower with a particular architectural profile via wind tunnel test. *Int. J. Archit. Herit.* **2021**, 1938748. [CrossRef]
12. Jiang, Y.; Li, A.; Xie, L.; Hou, M.; Qi, Y.; Liu, H. Development and application of an intelligent modeling method for ancient wooden architecture. *ISPRS Int. J. Geo-Inf.* **2020**, *9*, 167. [CrossRef]
13. Spear, M.J.; Broda, M. Comparison of contemporary elm (*Ulmus* spp.) and degraded archaeological elm: The use of dynamic mechanical analysis under ambient moisture conditions. *Materials* **2020**, *13*, 5026. [CrossRef]
14. Guo, J.; Zhou, H.; Stevanic, J.S.; Dong, M.; Yu, M.; Salmén, L.; Yin, Y. Effects of ageing on the cell wall and its hygroscopicity of wood in ancient timber construction. *Wood Sci. Technol.* **2018**, *52*, 131–147. [CrossRef]
15. Liang, R.; Zhu, Y.; Yang, X.; Gao, J.; Zhang, Y.; Cai, L. Study on the ultrastructure and properties of gelatinous layer in poplar. *J. Mater. Sci.* **2020**, *56*, 415–427. [CrossRef]
16. Lionetto, F.; Del Sole, R.; Cannoletta, D.; Vasapollo, G.; Maffezzoli, A. Monitoring wood degradation during weathering by cellulose crystallinity. *Materials* **2012**, *5*, 1910–1922. [CrossRef]
17. Pedersen, N.B.; Łucejko, J.J.; Modugno, F.; Björdal, C. Correlation between bacterial decay and chemical changes in waterlogged archaeological wood analysed by light microscopy and Py-GC/MS. *Holzforschung* **2021**, *75*, 635–645. [CrossRef]
18. Walsh-Korb, Z.; Avérous, L. Recent developments in the conservation of materials properties of historical wood. *Prog. Mater. Sci.* **2019**, *102*, 167–221. [CrossRef]
19. Irbe, I.; Bikovens, O.; Fridrihsone, V.; Dzenis, M. Impact of biodeterioration on structure and composition of waterlogged foundation piles from Riga Cathedral (1211 CE), Latvia. *J. Archaeol. Sci.* **2019**, *23*, 196–202. [CrossRef]
20. Broda, M.; Popescu, C.-M. The natural decay of archaeological oak wood versus artificial degradation processes—An FT-IR spectroscopy and X-ray diffraction study. *Spectrochim. Acta A Mol. Biomol. Spectrosc.* **2019**, *209*, 280–287. [CrossRef]
21. Bjurhager, I.; Halonen, H.; Lindfors, E.L.; Iversen, T.; Almkvist, G.; Gamstedt, E.K.; Berglund, L.A. State of degradation in archeological oak from the 17th century Vasa ship: Substantial strength loss correlates with reduction in (holo)cellulose molecular weight. *Biomacromolecules* **2012**, *13*, 2521–2527. [CrossRef] [PubMed]
22. Łucejko, J.J.; Tamburini, D.; Zborowska, M.; Babiński, L.; Modugno, F.; Colombini, M.P. Oak wood degradation processes induced by the burial environment in the archaeological site of Biskupin (Poland). *Herit. Sci.* **2020**, *8*, 44. [CrossRef]
23. Bader, T.K.; de Borst, K.; Fackler, K.; Ters, T.; Braovac, S. A nano to macroscale study on structure-mechanics relationships of archaeological oak. *J. Cult. Herit.* **2013**, *14*, 377–388. [CrossRef]
24. Sluiter, A.; Hames, B.; Ruiz, R.; Scarlata, C.; Sluiter, J.; Templeton, D.; Crocker, D. Determination of structural carbohydrates and lignin in biomass. *LAP* **2008**, *1617*, 1–16.
25. Segal, L.; Creely, J.J.; Martin, A.E.; Conrad, C.M. An empirical method for estimating the degree of crystallinity of native cellulose using the X-ray diffractometer. *Text. Res. J.* **1959**, *29*, 786–794. [CrossRef]
26. Oliver, W.C.; Pharr, G.M. An improved technique for determining hardness and elastic modulus using load and displacement sensing indentation experiments. *J. Mater. Res.* **1992**, *7*, 1564–1583. [CrossRef]
27. Jakes, J.E.; Stone, D.S. Best practices for quasistatic Berkovich nanoindentation of wood cell walls. *Forests* **2021**, *12*, 1696. [CrossRef]
28. Mayer, K.; Grabner, M.; Rosner, S.; Felhofer, M.; Gierlinger, N. A synoptic view on intra-annual density fluctuations in Abies alba. *Dendrochronologia* **2020**, *64*, 125781. [CrossRef]
29. Wang, D.; Lin, L.; Fu, F.; Fan, M. Fracture mechanisms of softwood under longitudinal tensile load at the cell wall scale. *Holzforschung* **2020**, *74*, 715–724. [CrossRef]

30. Monachon, M.; Albelda-Berenguer, M.; Lombardo, T.; Cornet, E.; Moll-Dau, F.; Schramm, J.; Schmidt-Ott, K.; Joseph, E. Evaluation of bio-based extraction methods by spectroscopic methods. *Minerals* **2020**, *10*, 203. [CrossRef]
31. Han, L.; Tian, X.; Keplinger, T.; Zhou, H.; Li, R.; Svedström, K.; Burgert, I.; Yin, Y.; Guo, J. Even visually intact cell walls in waterlogged archaeological wood are chemically deteriorated and mechanically fragile: A case of a 170 year-old shipwreck. *Molecules* **2020**, *25*, 1113. [CrossRef]
32. Guo, J.; Xiao, L.; Han, L.; Wu, H.; Yang, T.; Wu, S.; Yin, Y. Deterioration of the cell wall in waterlogged wooden archeological artifacts, 2400 years old. *IAWA J.* **2019**, *2*, 820–844. [CrossRef]
33. Xia, Y.; Chen, T.; Wen, J.; Zhao, Y.; Qiu, J.; Sun, R. Multi-analysis of chemical transformations of lignin macromolecules from waterlogged archaeological wood. *Int. J. Biol. Macromol.* **2018**, *109*, 407–416. [CrossRef]
34. Xu, K.; Gao, Y.; Zhang, X.; Li, Z.; Song, S.; Wu, Y.; Li, X.; Lu, J. Effects of drying temperature on hygroscopicity and mechanical performance of resin-impregnated wood. *Dry. Technol.* **2021**, *40*, 2414–2426. [CrossRef]
35. Zhou, Y.; Zhang, Y.; Zuo, Y.; Wu, Y.; Yuan, G.; Li, X. Construction of a network structure in Chinese fir wood by Na_2SiF_6 crosslinked Na_2SiO_3. *J. Mater. Res. Technol.* **2020**, *9*, 14190–14199. [CrossRef]
36. Zhou, Y.; Wang, Y.; Fan, M. Incorporation of tyre rubber into wood plastic composites to develop novel multifunctional composites: Interface and bonding mechanisms. *Ind. Crops Prod.* **2019**, *141*, 111788. [CrossRef]
37. Zhang, Y.; Yu, Y.; Lu, Y.; Yu, W.; Wang, S. Effects of heat treatment on surface physicochemical properties and sorption behavior of bamboo (Phyllostachys edulis). *Constr. Build. Mater.* **2021**, *282*, 122683. [CrossRef]
38. Yang, J.; Lu, X.; Zhang, Y.; Xu, J.; Yang, Y.; Zhou, Q. A facile ionic liquid approach to prepare cellulose fiber with good mechanical properties directly from corn stalks. *Green Energy Environ.* **2020**, *5*, 223–231. [CrossRef]
39. Liu, M.; Lyu, S.; Peng, L.; Lyu, J.; Huang, Z. Radiata pine fretboard material of string instruments treated with furfuryl alcohol followed by tung oil. *Holzforschung* **2021**, *75*, 480–493. [CrossRef]
40. Traore, M.; Kaal, J.; Martinez Cortizas, A. Variation of wood color and chemical composition in the stem cross-section of oak (*Quercus* spp.) trees, with special attention to the sapwood-heartwood transition zone. *Spectrochim. Acta A Mol. Biomol. Spectrosc.* **2023**, *285*, 121893. [CrossRef]
41. Xiao, M.; Chen, W.; Cao, X.; Chen, Y.; Zhao, B.; Jiang, Z.; Yuan, T.; Sun, R. Unmasking the heterogeneity of carbohydrates in heartwood, sapwood, and bark of Eucalyptus. *Carbohydr. Polym.* **2020**, *238*, 116212. [CrossRef] [PubMed]
42. Wang, T.; Liu, X.; Ma, C.; Wei, M.; Huo, P.; Yan, Y. In situ construction of $BiVO_4$(-)cellulose fibers@CDs(-)polyvinyl alcohol composites for tetracycline photocatalytic degradation. *Sci. China Tech. Sci.* **2020**, *64*, 548–558. [CrossRef]
43. Agarwal, U.P.; Ralph, S.A.; Baez, C.; Reiner, R.S.; Verrill, S.P. Effect of sample moisture content on XRD-estimated cellulose crystallinity index and crystallite size. *Cellulose* **2017**, *24*, 1971–1984. [CrossRef]
44. Yin, J.; Yuan, T.; Lu, Y.; Song, K.; Li, H.; Zhao, G.; Yin, Y. Effect of compression combined with steam treatment on the porosity, chemical compositon and cellulose crystalline structure of wood cell walls. *Carbohydr. Polym.* **2017**, *155*, 163–172. [CrossRef] [PubMed]
45. Guo, J.; Guo, X.; Wang, S.; Yin, Y. Effects of ultrasonic treatment during acid hydrolysis on the yield, particle size and structure of cellulose nanocrystals. *Carbohydr. Polym.* **2016**, *135*, 248–255. [CrossRef]
46. Dong, Y.; Altgen, M.; Mäkelä, M.; Rautkari, L.; Hughes, M.; Li, J.; Zhang, S. Improvement of interfacial interaction in impregnated wood via grafting methyl methacrylate onto wood cell walls. *Holzforschung* **2020**, *74*, 967–977. [CrossRef]
47. Zhang, Y.; Wang, Z.; Feng, J.; Pan, H. Maximizing utilization of poplar wood by microwave-assisted pretreatment with methanol/dioxane binary solvent. *Bioresour. Technol.* **2020**, *300*, 122657. [CrossRef]
48. Wang, D.; Lin, L.; Fu, F. The difference of creep compliance for wood cell wall CML and secondary S_2 layer by nanoindentation. *Mech. Time-Depend. Mater.* **2019**, *25*, 219–230. [CrossRef]
49. Konnerth, J.; Gierlinger, N.; Keckes, J.; Gindl, W. Actual versus apparent within cell wall variability of nanoindentation results from wood cell walls related to cellulose microfibril angle. *J. Mater. Sci.* **2009**, *44*, 4399–4406. [CrossRef]